MATHEMATICAL MODELING AND COMPUTING, Vol. 10, No. 4, pp. 1281–1291 (2023)

Haar wavelet collocation method for solving stagnation point flow over a nonlinearly stretching/shrinking sheet in a carbon nanotube with slip effect

Safian N. A. A.[1], Rasedee A. F. N[2], Bachok N.[1], Mahad Z.[3], Hasan M.[4]

[1]*Department of Mathematics and Statistics, Faculty of Science, University Putra Malaysia, 43400 Serdang, Selangor, Malaysia*
[2]*Faculty of Economics and Muamalat, University Sains Islam Malaysia, Malaysia*
[3]*Laboratory of Cryptography, Analysis and Structure, Institute for Mathematical Research, University Putra Malaysia, 43400 Serdang, Selangor, Malaysia*
[4]*Centre of Foundation Studies for Agricultural Science, University Putra Malaysia*

(Received 26 September 2023; Revised 21 November 2023; Accepted 22 November 2023)

This paper investigates the influence of slip effect on a stagnation point flow towards a shrinking/stretching sheet in carbon nanotube. The governing system of the partial differential equation is converted into a set of nonlinear ordinary differential equations by using a similarity transformation. The nonlinear ordinary differential equations are then solved numerically by Haar wavelets collocation method. The influence of the various parameters on the characteristics of the fluid flow and heat transfer is analyzed. Results are presented in terms of the skin friction coefficient and local Nusselt number, whereas the velocity and temperature profiles in the form of figures and thus, discussed in details.

Keywords: *Haar wavelet; stretching/shrinking sheet; MHD stagnation point flow; carbon nanotube.*

2010 MSC: 35B40, 76D05, 35Q30, 76D10, 76S05 **DOI:** 10.23939/mmc2023.04.1281

1. Introduction

Research on nonlinear stretching/shrinking sheet flow has appeared as a crucial element in a heat transfer research that concerns natural and engineering applications, such as in nanotechnology industries, metal forming, oil reservoir behavior, electronic cooling, coating and printing industry [1]. The original problem involving a continuously stretching sheet was pioneered by Sakiadis [2,3]. This classic problem, commonly referred to as "Sakiadis flow," has undergone extensive development to incorporate more intricate thermo-physical and geometric effects. Many researchers, among them Crane [4] and Gupta [5], have contributed to the extension and broadening the scope of this fundamental flow problem, delving into various factors that affect its behavior. Meanwhile, Bachok and Ishak [6] examined the flow around a nonlinear stretching/shrinking sheet within the stagnation region. They discovered non-unique solutions, particularly when the sheet was undergoing shrinking towards a fixed point. This discovery emphasized the intricate and multifaceted nature of the problem, wherein multiple distinct solutions can coexist under specific conditions. Furthermore, numerous researchers have acontributed to the exploration of nonlinear stretching/shrinking sheets, analyzing their behavior under various physical effects. Significantly, noteworthy contributions in this field have been made by Hayat et al. [7], Pal and Mandal [8], Rana et al. [9], Jamaludin et al. [10] and Reddy et al. [11]. Collectively, their work has provided valuable insights into the intricate dynamics of these systems, enriching our understanding of this complex area of study.

Nanofluids, were first introduced by Choi and Eastman [12], are defined as liquids containing dispersed submicron-sized solid particles, or nanoparticles. Among the various materials suitable for

This work was supported by Research Grant Putra, Universiti Putra Malaysia.

nanoparticle formation, carbon is particularly noteworthy due to its exceptional thermal, electrical, and mechanical properties [13]. Carbon nanotubes (CNTs) are a relatively recent and highly appealing class of carbon-based nanomaterials, characterized by their high aspect ratio. They are two main types of CNTs: Single-Wall Carbon Nanotubes (SWCNTs) and Multi-Wall Carbon Nanotubes (MWCNTs). In a study conducted by Choi et al. [14], focusing on oil-based carbon nanotubes (CNTs), it was observed that even a modest addition of nanotubes (1 vol%) led to a significant increase in the thermal conductivity of the base fluid. Garg et al. [15] explored the impact of dispersing energy on the viscous and heat transfer characteristics of MWCNTs dispersed in water. Their observation revealed a substantial 20% enhancement in thermal conductivity. Subsequently, numerous researchers have recognized the advantages of utilizing CNTs into their respective areas of study [16–18]. This underscores the promising role of CNTs in enhancing thermal properties and their broad applicability in various scientific and industrial domains.

Recently, the Haar wavelet collocation method (HWCM) has emerged as a significant and efficient technique for obtaining numerical solutions to differential and integro-differential equations. HWCM is a semi-numerical method that harnesses the unique properties of Haar wavelets. These wavelets are characterized by their piecewise constant functions, occurring in pairs, and they facilitate straightforward integration. Moreover, these orthogonal Haar functions form a basis foundation for transformation, making wavelets a valuable tool for analyzing dynamic phenomena, relevance in the engineering research. The pioneering use of Haar wavelets for solving systems of coupled ordinary differential equations (ODEs) related with boundary layer fluid problems, particularly involving high Prandtl numbers (Pr), was proposed by Sarler and Aziz [19]. This study highlights that the Haar wavelet collocation method (HWCM) surpasses traditional methods like the Runge–Kutta method (RKM) [20] and asymptotic techniques such as the Homotopy Analysis Method (HAM) [21]. The advantage of HWCM is its ability to directly address boundary value problems, directly without the need to convert them into initial value problems through shooting techniques. This direct approach enhances the stability of the method, especially when applied to problems with extensive computational domains, marking HWCM as a valuable tool for tackling complex boundary value problems in fluid dynamics. HWCM has been applied in solving two-dimensional boundary-layer flow problems in the presence of a uniform magnetic field. This approach has provided highly accurate solutions and revealed the occurrence of dual solutions for specific ranges of physical parameters Karkera et al. [22]. Subsequent research have consistently demonstrated the superior accuracy of Haar wavelets when compared to other numerical methods. These confirmatory studies have been conducted by researchers such as [23–25]. These findings collectively underscore the significance of Haar wavelets in numerical analysis and their potential to deliver highly precise results across various applications.

2. Haar wavelet

The one dimensional Haar wavelet family known as mother Haar wavelet for $x \in [0,1)$ can be described as

$$h_i(x) = \begin{cases} 1, & \text{for } x \in [\alpha, \beta), \\ -1, & \text{for } x \in [\beta, \gamma), \\ 0, & \text{elsewhere,} \end{cases}$$

where $\alpha = \frac{k}{m}$, $\beta = \frac{k+0.5}{m}$, $\gamma = \frac{k+1}{m}$. Integer m and k can be defined as $m = 2^j$, $j = 0, 1, \ldots, J$ that indicates the level of the wavelet while $k = 0, 1, \ldots, m-1$ is the translation parameter. J is the maximum level of resolution and index i is calculated by using the formula $i = m + k + 1$. For $i = 1$, function $h_1(x)$ is the scaling function which forms a square wave with unit magnitude stated as

$$h_1(t) = \begin{cases} 1, & t \in [0,1), \\ 0, & \text{elsewhere.} \end{cases}$$

By referring Karkera et al. [22], the integrals of the Haar functions are

$$P_{1,i}(t) = \int_0^t h_i(x)\,dx = \begin{cases} t-\alpha, & \text{for } t \in [\alpha,\beta), \\ \gamma - t, & \text{for } t \in [\beta,\gamma), \\ 0, & \text{elsewhere,} \end{cases}$$

$$P_{2,i}(t) = \int_0^t P_{1,i}(x)\,dx = \begin{cases} \frac{1}{2}(t-\alpha)^2, & \text{for } t \in [\alpha,\beta), \\ \frac{1}{4m^2} - \frac{1}{2}(\gamma - t)^2, & \text{for } t \in [\beta,\gamma), \\ \frac{1}{4m^2}, & \text{for} t \in [\gamma,1), \\ 0, & \text{elsewhere.} \end{cases}$$

Likewise, $P_{l+1,i}(t) = \int_0^t P_{l,i}(x)\,dx$, $l = 2, 3, \ldots$.

3. Methodology

Consider an incompressible steady flow in the region $y > 0$ driven by a stretching/shrinking surface located at $y = 0$ with a fixed stagnation point $x = 0$. The velocity of ambient fluid $U_\infty(x) = bx^n$ and stretching/shrinking $U_w(x) = ax^n$ are presumed to differ linearly from the stagnation point, where a and b are constant. Both SWCNTs and MWCNTs are used with water base fluid. The boundary layer equations can be defined as follows [26]

$$\frac{\partial u}{\partial x} + \frac{\partial v}{\partial y} = 0, \tag{1}$$

$$u\frac{\partial u}{\partial x} + v\frac{\partial u}{\partial y} = U_\infty \frac{dU_\infty}{dx} + \frac{\mu_{nf}}{\rho_{nf}}\frac{\partial^2 u}{\partial y^2}, \tag{2}$$

$$u\frac{\partial T}{\partial x} + v\frac{\partial T}{\partial y} = \alpha_{nf}\frac{\partial^2 T}{\partial y^2}, \tag{3}$$

and the boundary conditions are

$$\begin{gathered} u = U_w + L\frac{\partial u}{\partial y}, \quad v = V(x), \quad T = T_w + M\frac{\partial T}{\partial x} \quad \text{at} \quad y = 0, \\ u \to U_\infty, \quad T \to T_\infty \quad \text{as} \quad y \to \infty, \end{gathered} \tag{4}$$

where L and M denotes the slip factor where defined as $L = L_1 x^{\frac{-n+1}{2}}$ and $M = M_1 x^{\frac{-n+1}{2}}$ respectively. L_1 and M_1 is the slip factors initial length and $V(x)$ is the mass transfer velocity and T_w is the temperature of nanofluid. It should be mention that α_{nf}, $\mu_n f$, ρ_{nf}, $(\rho C_p)_{nf}$ and k_{nf} are the thermal diffusivity, viscosity, density, capacity of heat and thermal conductivity of nanofluid that Oztop and Abu Na-da [27] offer

$$\begin{gathered} \alpha_{nf} = \frac{k_{nf}}{(\rho C_p)_{nf}}, \quad \mu_{nf} = \frac{\mu_f}{(1-\varphi)^{2.5}}, \quad \rho_{nf} = (1-\varphi)\rho_f + \varphi\rho_{CNT}, \\ (\rho C_p)_{nf} = (1-\varphi)(\rho C_p)_f + \varphi(\rho C_p)_{CNT}, \\ \frac{k_{nf}}{k_f} = \frac{1 - \varphi + 2\varphi\frac{k_{CNT}}{k_{CNT}-k_f}\ln\frac{k_{CNT}+k_f}{2k_f}}{1 - \varphi + 2\varphi\frac{k_f}{k_{CNT}-k_f}\ln\frac{k_{CNT}+k_f}{2k_f}}, \end{gathered}$$

where φ is the CNTs volume fraction, $(\rho C_p)_{CNT}$, k_{CNT} and ρ_{CNT} are the capacity of heat, thermal conductivity and density of CNTs, and ρ_f and k_f are the density and thermal conductivity of the fluid. The use of the term for $\frac{k_{nf}}{k_f}$ was taken from the Maxwell's theory model that considers the effects of CNTs space distribution on thermal conductivity.

Equations (2) and (3) are reduced by the similarity transformation and the variables of similarity can be introduced as follows

$$\eta = \left(\frac{(n+1)b}{2v_f}\right)^{\frac{1}{2}} y\, x^{\frac{n-1}{2}}, \quad \psi = \left(\frac{2bv_f}{n+1}\right)^{\frac{1}{2}} x^{\frac{n+1}{2}} f(\eta), \quad \theta(\eta) = \frac{T-T_\infty}{T_w-T_\infty} \tag{5}$$

where η is the variable of similarity, ψ is the function of stream described as $u = \frac{\partial \psi}{\partial y}$ and $v = -\frac{\partial \psi}{\partial x}$ which comply with equation (1). Equations (2) and (3) can be reduced to these ODEs by using equation (5)

$$\frac{1}{(1-\varphi)^{2.5}\left(1-\varphi+\frac{\varphi\rho_{CNT}}{\rho_f}\right)} f''' + ff'' + \beta(1-f'^2) = 0, \tag{6}$$

$$\frac{1}{\mathrm{Pr}}\left[\frac{k_{nf}/k_f}{1-\varphi+\frac{\varphi(\rho C_p)_{CNT}}{(\rho C_p)_f}}\right]\theta'' + f\theta' = 0. \tag{7}$$

Thus, subject to the boundary condition equation (4) we have

$$\begin{gathered} f(0) = 0, \quad f'(0) = \varepsilon + \sigma f''(0), \quad \theta(0) = 1 + \sigma_t \theta'(0), \\ f'(\eta) \to 1, \quad \theta(\eta) \to 0 \quad \text{as} \quad \eta \to \infty, \end{gathered} \tag{8}$$

where $\beta = \frac{2n}{n+1}$ is the nonlinear parameter which varies from 1 to 2 as n grows from unity to infinity, $\varepsilon = a/b$ is the stretching/shrinking parameter where $\varepsilon < 0$ is shrinking $\varepsilon > 0$ is stretching, Prandtl number $\mathrm{Pr} = v_f/\alpha_f$, σ_t and σ are thermal slip and velocity parameter, respectively.

3.1. Numerical solution by Haar wavelet collocation method (HWCM)

The semi-infinites physical domain $[0, \infty)$ must be changed to suitable Haar wavelet context where it can be reduced to $[0, 1]$ by introducing the coordinate transformation $\xi = \eta/\eta_\infty$ and changing the variable to $F(\xi) = f(\eta)/\eta_\infty$ and $\theta_1(\xi) = \theta(\eta)/\eta_\infty$ to satisfy all the boundary conditions. Then, Equations (6) and (7) can be transformed to

$$\frac{1}{(1-\varphi)^{2.5}\left(1-\varphi+\frac{\varphi\rho_{CNT}}{\rho_f}\right)} F'''(\xi) + \eta_\infty^2 F(\xi)F''(\xi) + \beta\eta_\infty^2\left(1-(F'(\xi))^2\right) = 0, \tag{9}$$

$$\frac{1}{\mathrm{Pr}}\left[\frac{k_{nf}/k_f}{1-\varphi+\frac{\varphi(\rho C_p)_{CNT}}{(\rho C_p)_f}}\right]\theta_1''(\xi) + \eta_\infty^2 F(\xi)\theta_1'(\xi) = 0. \tag{10}$$

The boundary conditions of equation (3) are transformed to

$$\begin{gathered} F(0) = 0, \quad F'(0) = \varepsilon + \sigma\frac{F''(0)}{\eta_\infty}, \quad \theta_1(0) = \frac{1+\sigma_t\theta_1'(0)}{\eta_\infty}, \\ F'(\eta) \to 1, \quad \theta_1(\eta) \to 0 \quad \text{as} \quad \eta \to \eta_\infty. \end{gathered} \tag{11}$$

The higher order of derivatives for equations (9) and (10) are approximate by Haar wavelet,

$$F'''(\xi) = \sum_{i=1}^{2^{J+1}} a_i h_i(\xi), \tag{12}$$

$$\theta_1''(\xi) = \sum_{i=1}^{2^{J+1}} d_i h_i(\xi)\,. \tag{13}$$

The corresponding lower order of derivatives are derived using equation (12) and (13)

$$F''(\xi) = A(1-\varepsilon) + \sum_{i=1}^{2^{J+1}} a_i[P_{1,i}(\xi) - AC_i], \tag{14}$$

$$F'(\xi) = \varepsilon + A(1-\varepsilon)\left(\xi+\frac{\sigma}{\eta_\infty}\right) + \sum_{i=1}^{2^{J+1}} a_i\left[P_{2,i}(\xi) - A\left(\xi+\frac{\sigma}{\eta_\infty}\right)C_i\right], \tag{15}$$

$$F(\xi) = \xi\varepsilon + A(1-\varepsilon)\left(\frac{\xi^2}{2}+\frac{\xi\sigma}{\eta_\infty}\right) + \sum_{i=1}^{2^{J+1}} a_i\left[P_{3,i}(\xi) - A\left(\frac{\xi^2}{2}+\frac{\xi\sigma}{\eta_\infty}\right)C_i\right], \tag{16}$$

$$\theta_1'(\xi) = \sum_{i=1}^{2^{J+1}} d_i[P_{1,i}(\xi) - DC_i] - D, \tag{17}$$

$$\theta_1(\xi) = \sum_{i=1}^{2^{J+1}} d_i[P_{2,i}(\xi) - DC_i(\xi + \sigma_t)] - D(\xi + \sigma_t) + 1, \tag{18}$$

where

$$C_i = \int_0^1 P_{1,i}(t)\,dt, \qquad A = \frac{\eta_\infty}{\sigma + \eta_\infty}, \qquad D = \frac{\eta_\infty}{\sigma_t + 1},$$

Then, equations (14)–(18) are substituted into equations (9) and (10). By applying collocation point,

$$\xi_l = \frac{1}{2^{J+1}}\left(l - \frac{1}{2}\right), \quad l = 1, 2, \ldots, 2^{J+1},$$

we obtain numerical solutions for the ODEs to system nonlinear equations with 2^{J+1} unknown wavelet coefficients.

3.2. Method of solution

In this research, the quantities of physical interest are the Nusselt number Nu_x and the coefficient of skin friction C_f, given by Malvandi et al. [28]:

$$\mathrm{Nu}_x = \frac{xq_w}{k_f(T_w - T_\infty)}, \quad C_f = \frac{\tau_w}{\rho_f U_\infty^2},$$

in which the surface heat flux q_w and the surface shear stress τ_w are likely identified as

$$q_w = -k_{nf}\left(\frac{\partial T}{\partial y}\right)_{y=0}, \quad \tau_w = \mu_{nf}\left(\frac{\partial u}{\partial y}\right)_{y=0}$$

with k_{nf} is the thermal conductivity of the nanofluids and μ_{nf} is the viscosity of the nanofluids. Physical interests that we acquire after the transformation are

$$C_f\,\mathrm{Re}_x^{\frac{1}{2}} = \frac{1}{(1-\varphi)^{2.5}}\sqrt{\frac{1}{2-\beta}}f''(0), \tag{19}$$

$$\frac{\mathrm{Nu}_x}{\mathrm{Re}_x^{\frac{1}{2}}} = -\frac{k_{nf}}{k_f}\sqrt{\frac{1}{2-\beta}}\theta'(0), \tag{20}$$

where

$$\mathrm{Re}_x = \frac{U_\infty x}{v_f}, \qquad f''(0) = A(1-\varepsilon) - A\sum_{i=1}^{2^{J+1}} a_i C_i, \qquad \theta'(0) = -D\sum_{i=1}^{2^{J+1}} d_i C_i - D.$$

4. Results & discussions

The ODEs (9) and (10) with boundary conditions (11) are solved and obtained the numerical solutions via Maple Software. Water is used as the base fluid for both SWCNTs and MWCNTs. By following Norzawary et al. [29], the selection of φ is $0 \leqslant \varphi \leqslant 0.2$, where $\varphi = 0$ is regular fluid with $\mathrm{Pr} = 6.2$ (water). The researchers also mentioned the base fluid's and CNTs' thermophysical properties as shown in Table 1.

Table 1. Thermophysical properties of CNTs.

Physical properties	Base fluids	Nanoparticle	
		SWCNT	MWCNT
ρ (kg/m^3)	997	2600	1600
c_p (J/kg K)	4179	425	796
k (W/mK)	0.163	6600	3000

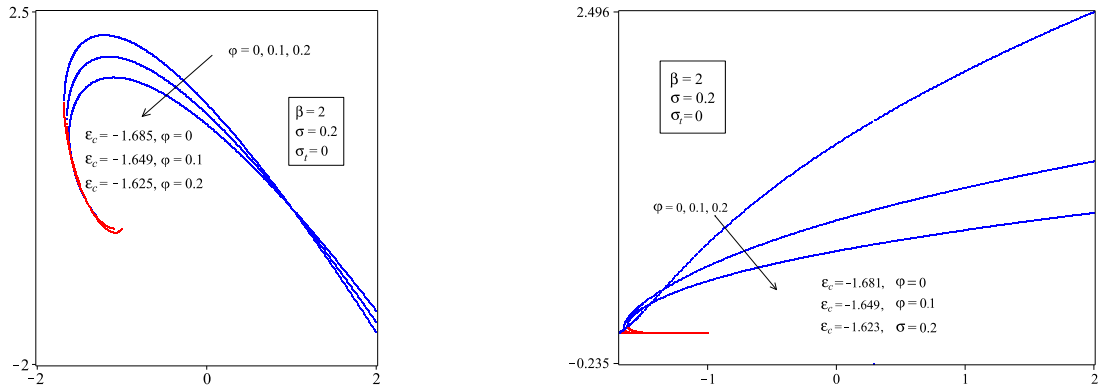

a $(f''(0))$ ***b*** $(-\theta'(0))$

Fig. 1. $f''(0)$ and $-\theta'(0)$ with ε and φ for water–SWCNTs.

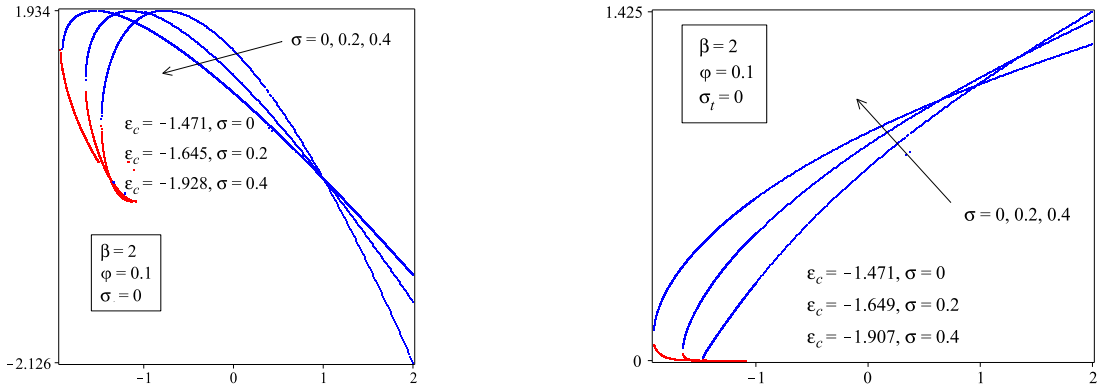

a $(f''(0))$ ***b*** $(-\theta'(0))$

Fig. 2. $f''(0)$ and $-\theta'(0)$ with ε and σ for water–SWCNTs.

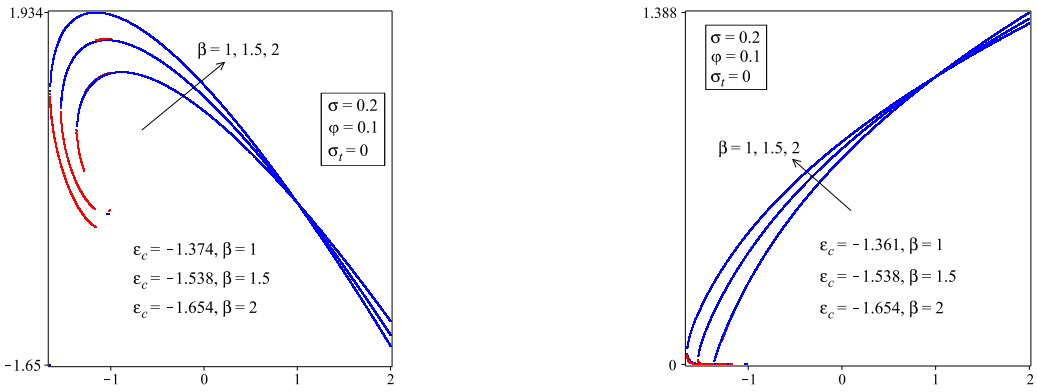

a $(f''(0))$ ***b*** $(-\theta'(0))$

Fig. 3. $f''(0)$ and $-\theta'(0)$ with ε and β for water–SWCNTs.

Figures $1a$ and $1b$ show the $f''(0)$ and $-\theta'(0)$ graphs for some values of stretching/shrinking parameter ε and different values of φ when $\mathrm{Pr} = 6.2$ for water–SWCNTs. Both figures show that we obtained a unique solution when $\varepsilon > -1$, dual solutions when $\varepsilon_c < \varepsilon \leqslant -1$, and no solutions when $\varepsilon < \varepsilon_c$. Next, Figures $2a$ and $2b$ present the $f''(0)$ and $-\theta'(0)$ graphs for some values of ε and different values of velocity slip parameter σ for water–SWCNTs. Both graphs show that the range of ε values where the solution exists get bigger $(\varepsilon \geqslant \varepsilon_c)$ when σ increases at the boundary.

Figures $3a$ and $3b$ illustrate the $f''(0)$ and $-\theta'(0)$ graph for certain values of ε and three different values of β which are $\beta = 1, 1.5$ and 2 for water base fluid when $\varphi = 0.1$ and $\sigma = 0.2$. Both graphs conclude that the range of solutions given by β is bigger compared to φ and σ. This also shows that the boundary layer separation is postponed when the values of β increase.

Figures 4a and 4b show the $\mathrm{Nu}_x(\mathrm{Re}_x)^{-1/2}$ and $C_f(\mathrm{Re}_x)^{1/2}$ as functions of Reynolds number, given by the equations (19) and (20) using φ and σ with set $\varepsilon = 0.5$. It can be concluded that the coefficient of skin friction decreases while the local Nusselt number increases when σ increases. The presence of slip enhances the convective heat transfer on the surface. By referring to Table 1, since SWCNTs have higher density and thermal conductivity than MWCNTs, result in elevated values for both $C_f(\mathrm{Re}_x)^{1/2}$ and $\mathrm{Nu}_x(\mathrm{Re}_x)^{-1/2}$. Moving on to Figures 5$a$ and 5b illustrate various β for $\mathrm{Nu}_x(\mathrm{Re}_x)^{-1/2}$ and $C_f(\mathrm{Re}_x)^{1/2}$. These figures show that both $\mathrm{Nu}_x(\mathrm{Re}_x)^{-1/2}$ and $C_f(\mathrm{Re}_x)^{1/2}$ increase when β increases, displaying a clear linear correlation with φ.

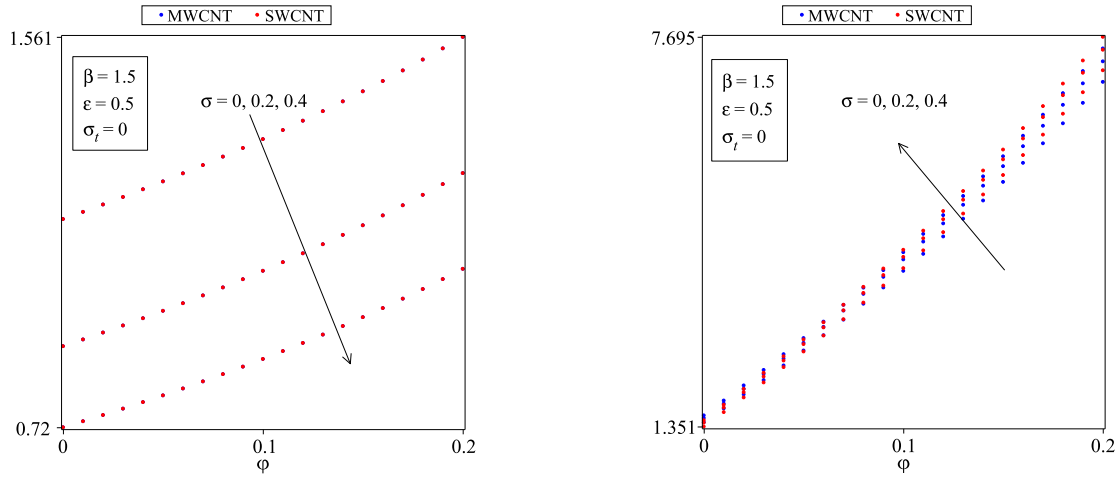

a $(C_f(\mathrm{Re}_x)^{1/2})$ ***b*** $(\mathrm{Nu}_x(\mathrm{Re}_x)^{-1/2})$

Fig. 4. Variation of $C_f(\mathrm{Re}_x)^{1/2}$ and $\mathrm{Nu}_x(\mathrm{Re}_x)^{-1/2}$ with φ and σ for water base fluid.

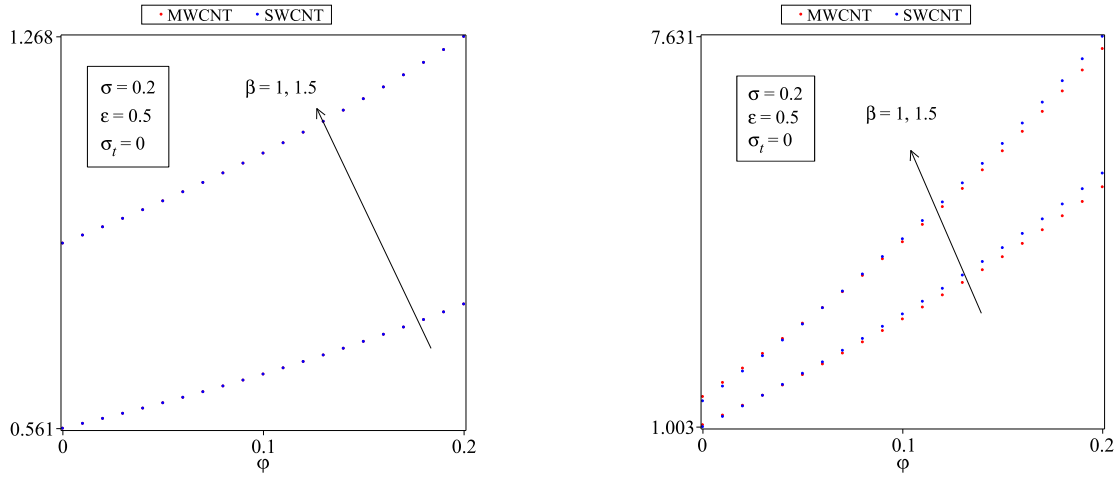

a $(C_f(\mathrm{Re}_x)^{1/2})$ ***b*** $(\mathrm{Nu}_x(\mathrm{Re}_x)^{-1/2})$

Fig. 5. Variation of $C_f(\mathrm{Re}_x)^{1/2}$ and $\mathrm{Nu}_x(\mathrm{Re}_x)^{-1/2}$ with φ and β for water base fluid.

The velocity and temperature profiles for different values of φ for water–SWCNTs are shown in Figures 6a and 6b. It can be seen clearly that $\theta(\eta)$ increases within thermal boundary layer thickness and $f''(\eta)$ decreases within the momentum boundary layer when φ increases. Figures 7a and 7b show the velocity and temperature profiles for various values of σ for water–SWCNTs. For both solutions, $f'(\eta)$ increases within the momentum boundary layer thickness when σ increases, while $\theta(\eta)$ decreases leading to a reduction in the thermal boundary layer thickness. Lastly, Figures 8a and 8b display the velocity and temperature profiles for different values of β. Both figures show that $f'(\eta)$ increases within momentum boundary layer thickness, while $\theta(\eta)$ decreases within thermal boundary layer thickness for both the first and second solutions.

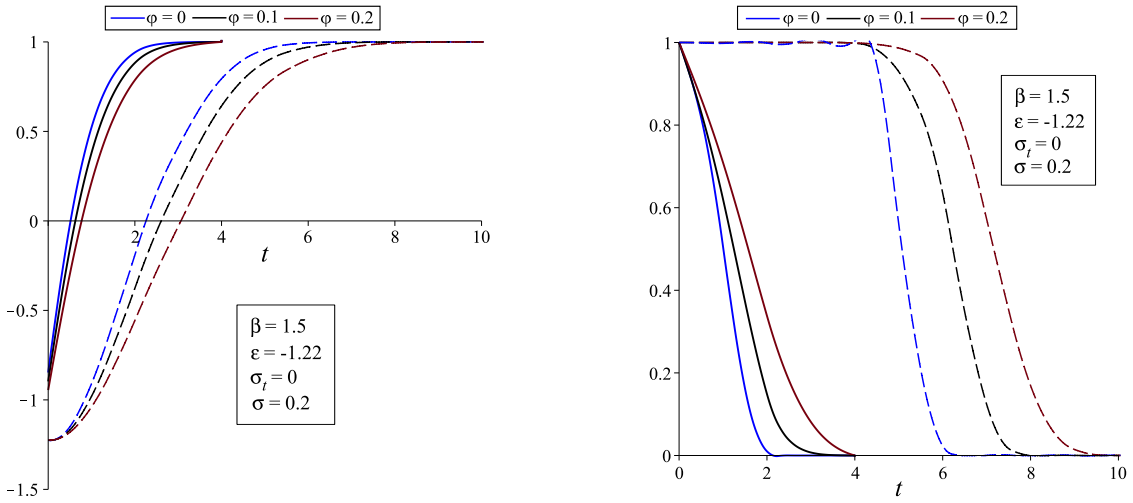

a (Velocity profile) ***b*** (Temperature profile)

Fig. 6. Velocity and temperature profile for φ and water–SWCNTs.

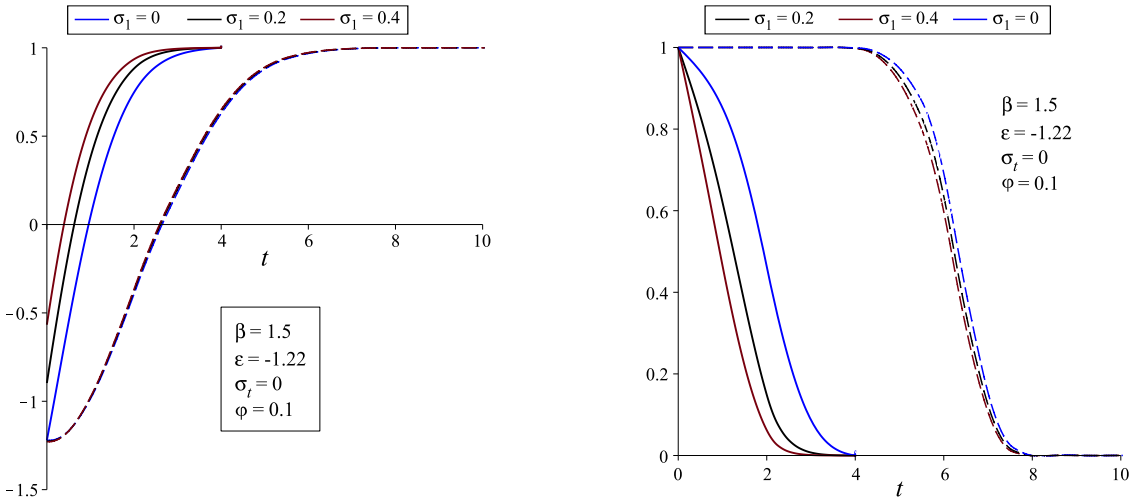

a (Velocity profile) ***b*** (Temperature profile)

Fig. 7. Velocity and temperature profile for σ and water–SWCNTs.

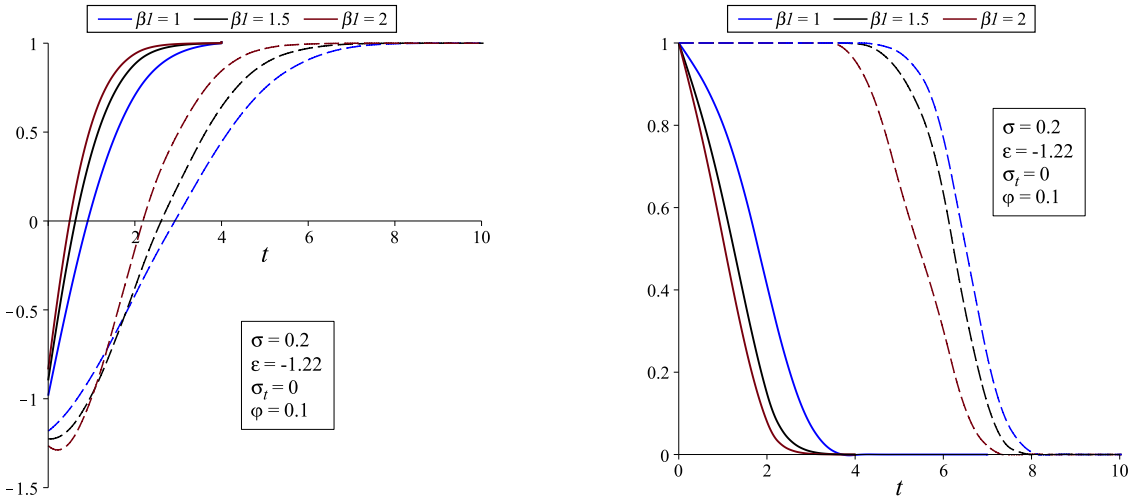

a (Velocity profile) ***b*** (Temperature profile)

Fig. 8. Velocity and temperature profile for β and water–SWCNTs.

5. Conclusion

This research analyzed the numerical study for the stagnation point flow over a nonlinearly stretching or shrinking surface in CNTs with slip effects. The numerical solution is obtained using the Haar wavelet method in Maple software.

— It can be concluded that a unique solution exists when $\varepsilon > -1$, while dual solutions exist when $\varepsilon_c < \varepsilon \leqslant -1$ and no solutions are found to exist when $\varepsilon < \varepsilon_c$ (ε_c is critical value of ε). Additionally, it is established that shrinking sheet result in dual solutions while stretching sheet yields unique solutions.

— Furthermore, the study explores various parameters, including CNTs volume fraction φ, velocity slip parameter σ, thermal slip parameter σ_t and nonlinear parameter β. In this problem, raising φ speeds up boundary layer separations while higher values of σ and β broaden the range of solutions, implying that these parameters delay boundary layer separation.

— Additionally, as φ increases, the skin friction and Nusselt number are continuously increasing. Moreover, SWCNTs outperform MWCNTs in terms of skin friction and local Nusselt number due to their superior thermal conductivity.

[1] Yu B., Chiu H.-T., Ding Z., Lee L. J. Analysis of flow and heat transfer in liquid composite molding. International Polymer Processing. **15** (3), 273–283 (2000).

[2] Sakiadis B. C. Boundary-layer behavior on continuous solid surfaces: I. Boundary-layer equations for two-dimensional and axisymmetric flow. AIChE Journal. **7** (1), 26–28 (1961).

[3] Sakiadis B. C. Boundary-layer behavior on continuous solid surfaces: II. The boundary layer on a continuous flat surface. AiChE journal. **7** (2), 221–225 (1961).

[4] Crane L. J. Flow past a stretching plate. Zeitschrift für angewandte Mathematik und Physik ZAMP. **21**, 645–647 (1970).

[5] Gupta P. S., Gupta A. S. Heat and mass transfer on a stretching sheet with suction or blowing. The Canadian Journal of Chemical Engineering. **55** (6), 744–746 (1977).

[6] Bachok N., Ishak A. Similarity solutions for the stagnation-point flow and heat transfer over a nonlinearly stretching/shrinking sheet. Sains Malaysiana. **40** (11), 1297–1300 (2011).

[7] Hayat T., Aziz A., Muhammad T., Alsaedi A. On magnetohydrodynamic three-dimensional flow of nanofluid over a convectively heated nonlinear stretching surface. International Journal of Heat and Mass Transfer. **100**, 566–572 (2016).

[8] Pal D., Mandal G. Double diffusive magnetohydrodynamic heat and mass transfer of nanofluids over a nonlinear stretching/shrinking sheet with viscous–Ohmic dissipation and thermal radiation. Propulsion and Power Research. **6** (1), 58–69 (2017).

[9] Rana P., Dhanai R., Kumar L. Radiative nanofluid flow and heat transfer over a non-linear permeable sheet with slip conditions and variable magnetic field: Dual solutions. Ain Shams Engineering Journal. **8** (3), 341–352 (2017).

[10] Jamaludin A., Nazar R., Pop I. Three-dimensional magnetohydrodynamic mixed convection flow of nanofluids over a nonlinearly permeable stretching/shrinking sheet with velocity and thermal slip. Applied Sciences. **8** (7), 1128 (2018).

[11] Reddy N. V. B., Kishan N., Reddy C. S. Melting heat transfer and MHD boundary layer flow of Eyring–Powell nanofluid over a nonlinear stretching sheet with slip. International Journal of Applied Mechanics and Engineering. **24** (1), 161–178 (2019).

[12] Chol S. Enhancing thermal conductivity of fluids with nanoparticles. ASME-Publications-Fed. Vol. 231 (1995).

[13] Halelfadl S., Maré T., Estellé P. Efficiency of carbon nanotubes water based nanofluids as coolants. Experimental Thermal and Fluid Science. **53**, 104–110 (2014).

[14] Choi S. U. S., Zhang Z. G., Yu W., Lockwood F. E., Grulke E. A. Anomalous thermal conductivity enhancement in nanotube suspensions. Applied Physics Letters. **79** (14), 2252–2254 (2001).

[15] Garg P., Alvarado J. L., Marsh C., Carlson T. A., Kessler D. A., Annamalai K. An experimental study on the effect of ultrasonication on viscosity and heat transfer performance of multi-wall carbon nanotube-based aqueous nanofluids. International Journal of Heat and Mass Transfer. **52** (21–22), 5090–5101 (2009).

[16] Xue Q. Z. Model for thermal conductivity of carbon nanotube-based composites. Physica B: Condensed Matter. **368** (1–4), 302–307 (2005).

[17] Ding Y., Alias H., Wen D., Williams R. A. Heat transfer of aqueous suspensions of carbon nanotubes (CNT nanofluids). International Journal of Heat and Mass Transfer. **49** (1–2), 240–250 (2006).

[18] Kumaresan V., Velraj R., Das S. K. Convective heat transfer characteristics of secondary refrigerant based CNT nanofluids in a tubular heat exchanger. International Journal of Refrigeration. **35** (8), 2287–2296 (2012).

[19] Siraj-ul-Islam, Šarler B., Aziz I., Fazal-I-Haq. Haar wavelet collocation method for the numerical solution of boundary layer fluid flow problems. International Journal of Thermal Sciences. **50** (5), 686–697 (2011).

[20] Na T. Y. (Ed.). Computational Methods in Engineering Boundary Value Problems. Academic Press (1979).

[21] Liao S. J. The proposed homotopy analysis technique for the solution of nonlinear problems. Doctoral dissertation, PhD thesis, Shanghai Jiao Tong University (1992).

[22] Karkera H., Katagi N. N., Kudenatti R. B. Analysis of general unified MHD boundary-layer flow of a viscous fluid – a novel numerical approach through wavelets. Mathematics and Computers in Simulation. **168**, 135–154 (2020).

[23] Sathar M. H. A., Rasedee A. F. N., Ahmedov A. A., Bachok N. Numerical solution of nonlinear Fredholm and Volterra integrals by Newton–Kantorovich and Haar wavelets methods. Symmetry. **12** (12), 2034 (2020).

[24] Awati V. B., Kumar M., Wakif A. Haar wavelet scrutinization of heat and mass transfer features during the convective boundary layer flow of a nanofluid moving over a nonlinearly stretching sheet. Partial Differential Equations in Applied Mathematics. **4**, 100192 (2021).

[25] Karkera H., Katagi N. N. Haar wavelet collocation method for the investigation of micropolar fluid flow in a porous channel with suction and injection. International Journal of Mathematical Modelling and Numerical Optimisation. **12** (2), 157–175 (2022).

[26] Ahmad S. , Rohni A. M., Pop I. Blasius and Sakiadis problems in nanofluids. Acta Mechanica. **218**, 195–204 (2011).

[27] Oztop H. F., Abu-Nada E. Numerical study of natural convection in partially heated rectangular enclosures filled with nanofluids. International Journal of Heat and Fluid Flow. **29** (5), 1326–1336 (2008).

[28] Malvandi A., Hedayati F., Ganji D. D. Nanofluid flow on the stagnation point of a permeable non-linearly stretching/shrinking sheet. Alexandria engineering journal. **57** (4), 2199–2208 (2018).

[29] Norzawary N. H. A., Bachok N., Ali F. M. Effects of Suction/Injection on Stagnation Point Flow over a Nonlinearly Stretching/Shrinking Sheet in a Carbon Nanotubes. Journal of Advanced Research in Fluid Mechanics and Thermal Sciences. **76** (1), 30–38 (2020).

Метод вейвлет-колокації Хаара для розв'язування задачі точки застою потоку по листі, який нелінійно розтягується/стискається, у вуглецевій нанотрубці з ефектом ковзання

Сафіян Н. А. А.[1], Раседі А. Ф. Н.[2], Бачок Н.[1], Махад З.[3], Хасан М.[4]

[1] *Кафедра математики та статистики, факультет природничих наук, Університет Путра Малайзії, 43400 Серданг, Селангор, Малайзія*
[2] *Факультет економіки та Муамалат, Университет Сайнс Ісламм Малайзія, Малайзія*
[3] *Лабораторія криптографії, аналізу та структури, Інститут математичних досліджень, Університет Путра Малайзії, 43400 Серданг, Селангор, Малайзія*
[4] *Центр фундаментальних досліджень сільськогосподарської науки, Університет Путра Малайзії*

У цій статті досліджується вплив ефекту ковзання на потік в точці застою по листі, який стискається/розтягується, у вуглецевій нанотрубці. Основна система рівняння в частинних похідних перетворюється на набір нелінійних звичайних диференціальних рівнянь за допомогою перетворення подібності. Потім нелінійні звичайні диференціальні рівняння розв'язуються чисельним способом методом колокації вейвлетів Хаара. Проведено аналіз впливу різних параметрів на характеристики потоку рідини та перенесення тепла. Результати представлені в термінах коефіцієнта поверхневого тертя та локального числа Нуссельта, тоді як профілі швидкості та температури подано на графіках та детально обговорені.

Ключові слова: *вейвлет Хаара; лист, що розтягується/стискається; МГД потік точки застою; вуглецева нанотрубка.*